β-Ga_2O_3 and single-crystal phosphors for high-brightness white LEDs & LDs, and β-Ga_2O_3 potential for next generation of power devices

Encarnación G. Víllora[a], Stelian Arjoca[a,b] and Kiyoshi Shimamura[a,b]
Daisuke Inomata[c] and Kazuo Aoki[c]

[a]National Institute for Materials Science, 1-1 Namiki, Tsukuba 305-0044, Japan;
[b]Graduate School of Advanced Science and Engineering, Waseda University, 3-4-1 Okubo, Shinjuku, Tokyo 169-8555, Japan;
[c]KOHA Co., Ltd., Nerima, Tokyo 176-0022, Japan

ABSTRACT

β-Ga_2O_3 is the most transparent conductive oxide, well known since several decades for its large bandgap of 4.8 eV. Its potential as semiconductor material, however, is just emerging in recent years. Present work shows the development of β-Ga_2O_3 for semiconductor applications and its current state-of-the-art. The discussion is focused on three different aspects: (1) Advantageous growth from melt of large-size β-Ga_2O_3 single-crystals. High-crystalline quality and carrier control make possible the production of conductive and semi-insulating wafers. (2) β-Ga_2O_3 as substrate for homoepitaxy as well as for heteroepitaxial deposition of GaN-based devices. High-brightness blue-LEDs with vertical current injection are demonstrated. (3) Potential of β-Ga_2O_3 for high-power devices with higher breakdown voltage than GaN and SiC counterparts. The first Schottky barrier diode is shown, as well as first transistors (MESFET and MOSFET) are indicated.

Single-crystal phosphors are introduced as novel alternative to currently used powder phosphors. In connection with high-brightness white light-sources, based on LEDs or LDs plus phosphor converters, single-crystal phosphors possess advantageous features. These avoid the use of resins and exhibit a very high internal quantum efficiency, which remains stable with the temperature increase.

Keywords: β-Ga_2O_3 crystal growth, single-crystal phosphors, GaN heteroepitaxy, high-brightness white LEDs, high-power devices

1. INTRODUCTION

β-Ga_2O_3 is a wide bandgap oxide known for many decades. However, only in the recent years there has been an emerging interest on this n-type semiconductor. There are probably two major reasons that accounted for the disregard of this oxide. On the one hand, its crystal structure differs largely from that of other standard semiconductors, as well from that of other oxides in the same IIIA group, Al_2O_3 and In_2O_3. So, the lattice mismatch and the difficulties for bandgap engineering were evident. On the other hand, it was quite difficult to grow high-quality large single-crystals that could be cut and polished into wafers. In spite of all these issues, nowadays there is an increasing demand on the supply of β-Ga_2O_3 wafers for different types of semiconductor applications, including GaN-family heteroepitaxy as well as homoepitaxy. β-Ga_2O_3 compromises the characteristic properties of the two standard substrates for GaN-based light-emitting diodes (LEDs), namely the visible transparency of sapphire and the conductivity of SiC. Therefore, β-Ga_2O_3 is an attractive substrate for the fabrication of efficient high-brightness vertically-structured LEDs. Another relevant application of β-Ga_2O_3 is the next generation of power devices. The wide bandgap of β-Ga_2O_3 E_g=4.8 eV is very promising to achieve a very high breakdown voltage. Two of the important issues remaining on the development of β-Ga_2O_3 is the observation of band-edge emission and the p-type doping, which would drastically broaden the application fields. For example, the first deep UV LEDs and laser diodes (LDs) could be produced.

E-mail:villora.garcia@nims.go.jp

Oxide-based Materials and Devices V, edited by Ferechteh H. Teherani, David C. Look, David J. Rogers, Proc. of SPIE Vol. 8987, 89871U · © 2014 SPIE
CCC code: 0277-786X/14/$18 · doi: 10.1117/12.2039305

The first part of this work is devoted to the β-Ga_2O_3 development. Special emphasis is put on the main achievements that have taken place recently. These can be divided into three topics: One is the growth of large single-crystals of high crystalline quality and the control of carrier concentration. Another is the understanding of GaN heteroepitaxy and the fabrication of high-brightness LEDs. And the last is the first demonstration of high breakdown-voltage Schottky barrier diodes and transistors, indicating the potential of β-Ga_2O_3 for high-voltage high-power devices.

The second part deals with the development of other oxides as single-crystal phosphors. These, in connection with high-brightness LEDs or LDs, can guarantee efficient and long-lasting white light-sources for general illumination purposes. It will be shown that single-crystal phosphors exhibit not only higher internal quantum efficiencies (QEs), but also an outstanding temperature stability in comparison with currently used powder phosphors embedded in resins.

2. β-Ga_2O_3 AS "NEW" SEMICONDUCTOR MATERIAL

2.1 β-Ga_2O_3 growth and properties

Among the reported Ga_2O_3 polymorphs (α, γ, δ, ε, and β), only the last modification is stable under any temperature and conditions. The crystal structure of β-Ga_2O_3 was elucidated in 1960.[1] It belongs to the monoclinic system, with space group $C2/m$ (C_{2h}^3). The unit cell is illustrated in Fig.1 (left). It contains four formula units, which are distributed evenly in two cation and three anion sites. The Ga octahedral-chains share edges along the *b*-axis, while the Ga tetrahedral-chain shares only corners. The symmetry is very low, presenting only a 2-fold symmetry around the *b*-axis. Further, as it has center of symmetry, it lacks special properties like polarity, piezoelectricity, ferroelectricity, etc.

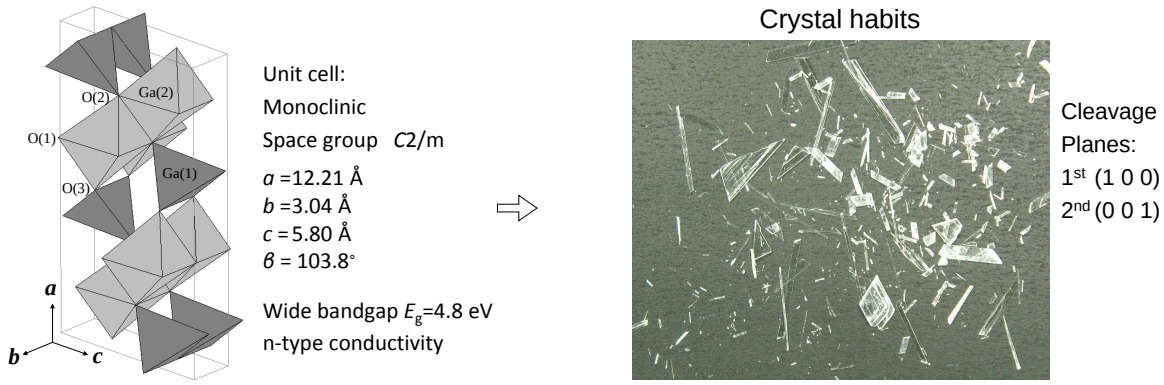

Figure 1. (left) Schematic of the β-Ga_2O_3 unit cell, showing the two gallium locations in octahedral and tetrahedral sites. (right) Typical needle- and platelet-like habits of this compound.

β-Ga_2O_3 possesses two cleavage planes, the main (1 0 0) and the secondary (0 0 1). These planes with weak bonding character determine the fragility and typical crystal habits observed: needles and plates (Fig.1 (right)). The preferential growth along the *b*-axis is responsible for the multiple reports on milimeter- to micrometer-sized β-Ga_2O_3 crystals, denominated as "nano"-rods, -wires, -ribbons, -belts, etc. Crystallites exhibit in general a high crystalline quality. With the increase in size, however, β-Ga_2O_3 has a strong tendency to present microtwinning, meaning with it a random variation of the crystal direction in the order of degrees. This is the origin of the apparent fragility of crystals during cutting, breaking like mica, and it has for long time hampered the processing of crystals into a desired shape and direction.

Apart from the crystal structure, the growth of β-Ga_2O_3 single-crystals presents two additional difficulties. The first one is its high melting point, 1725℃, and the second is its reductive decomposition ($Ga_2O_3 \rightarrow Ga_2O + O_2$) and the subsequent high vapor pressure associated to its components. The growth of β-Ga_2O_3 from melt requires the use of an iridium crucible, which is gradually attacked by the corrosive melt. In order to avoid the use of Ir-crucible and to control the evaporation better by an atmosphere containing O_2, the floating

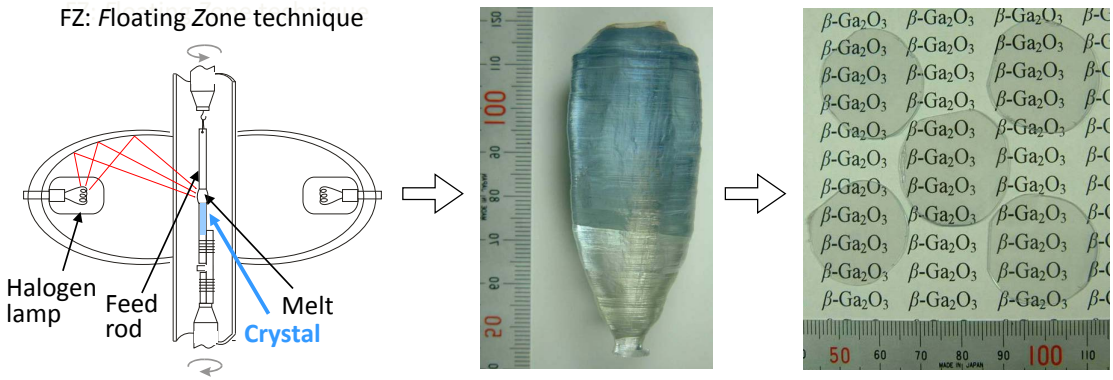

Figure 2. (left) Schematic of the floating zone technique, which avoids the use of Ir-crucibles. (right) A β-Ga_2O_3 single crystal over 1 inch in diameter and the wafers obtained from it.

zone (FZ) technique is used at first (see schematic of Fig. 2). By this technique it has been shown that the growth along the crystallographic axes is more stable, thus these favor the growth of crack-free large-size single crystals.[2] Taking into account the cleavage nature, the growth along the <0 1 0>direction is preferred. Due to the improved crystallinity it was possible for the first time to cut and polish single crystals into wafers of any desired orientation. Figure 2 shows the first crystal with a diameter over 1 inch and the (1 0 0) wafers produced from it.

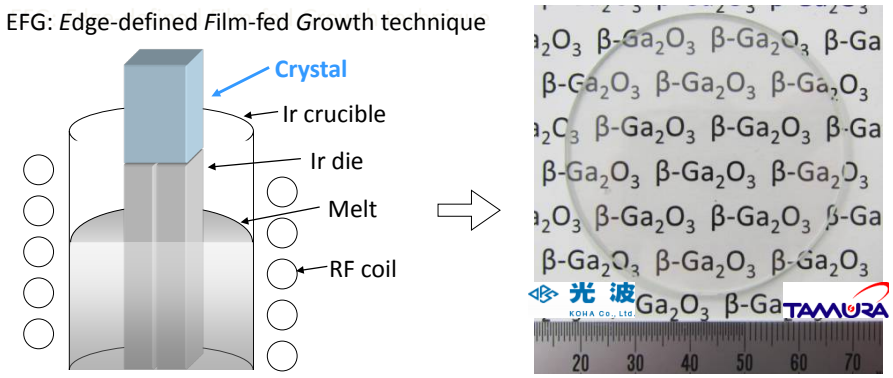

Figure 3. (left) Schematic of the EFG technique, based on capillary melt rise. (right) A standard 2 inch ($\bar{2}$ 0 1) β-Ga_2O_3 single-crystal wafer produced nowadays industrially by KOHA Co., Ltd. & Tamura Corp. using the EFG technique.

Though the FZ technique was very useful for laboratory-scale studies, this technique is limited to crystals of 1 inch due to the optical heating. In order to increase the size to 2 inch, which is the minimum diameter required for industrial production, it was necessary to switch to the EFG (*E*dge-defined *F*ilm-fed *G*rowth) technique. Although this method is less known than the most common Czochralki (Cz) technique, it is widely used for the growth of shaped crystals like *e.g.* sapphire. Figure 3 (left) shows schematically the growth principle, based on a crucible with a die and the melt rising up through the capillary effect. This method is very convenient for the growth of high quality β-Ga_2O_3 single crystals. In this case, although Ir is used as a crucible, the Ir-particles floating on the melt surface do not disturb the growth process. Crystals can be pulled up at a higher speed, 10-30 mm/h, with a comparatively lower energy consumption and a lower waste of raw-materials than *e.g.* the case of Cz technique. Also, as the crystals are not rotated, the growth interface is very stable and the twinning tendency is suppressed. By this technique, 2 inch wafers as the one shown in Fig. 3 (right) are produced by KOHA Co., Ltd. & Tamura Corp. Another favorable feature of this technique is its scalability, being feasible for the growth of crystals of several inches. Therefore, a continuous decrease in production costs is expected, leading with it to very competitive prices in comparison with GaN and SiC counterparts.

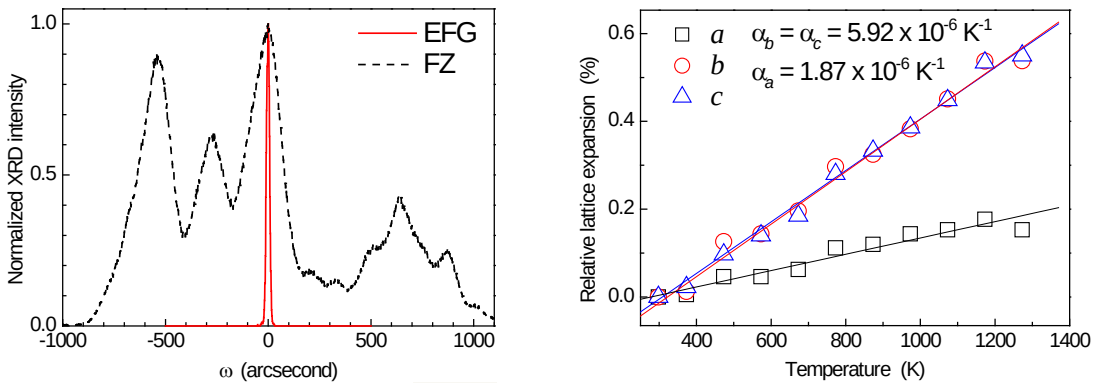

Figure 4. (left) X-ray rocking curve of the (4 0 0) reflection from a FZ-wafer in comparison with that of the ($\bar{2}$ 0 1) reflection from the best EFG-wafer. (right) Linear expansion coefficients of β-Ga_2O_3 along the three crystallographic axes.

The crystalline quality of β-Ga_2O_3 crystals grown by the FZ and EFG techniques is compared in Fig. 4 (left). Although in $\theta/2\theta$ scans of *e.g.* an *a*-plane FZ-wafer single {1 0 0} reflections are observed, the rocking curve can present a few overlapping peaks of about 200 arcsec FWHM. This indicates the existence of the above mentioned micro-twinning. In contrast, twin-free wafers can be produced by the EFG technique, exhibiting FWHM below 350 arcsec. The rocking curve of the best ($\bar{2}$ 0 1) wafer, with a FWHM as narrow as 19 arcsec, proves the high crystalline quality already achieved by the EFG technique. Further, the etch pit density of these wafers, after 120 min. in phosphoric acid at 120℃, is as low as 10^4 cm^{-2}.

The use of β-Ga_2O_3 wafers for heteroepitaxial purposes depends on lattice mismatch, thermal expansion coefficient and electrical properties. The first issue is discussed in detail in section 2.2 for the case of GaN epitaxy. The linear expansion coefficients have been determined from the measurements shown in Fig. 4 (right). The coefficients along the *b*- and *c*-axes are the same, with a value of 5.9×10^{-6} K^{-1}. The homogeneous in-plane expansion of the *a*-plane contrasts with the about three times smaller expansion coefficient along the *a*-axis (1.9×10^{-6} K^{-1}).

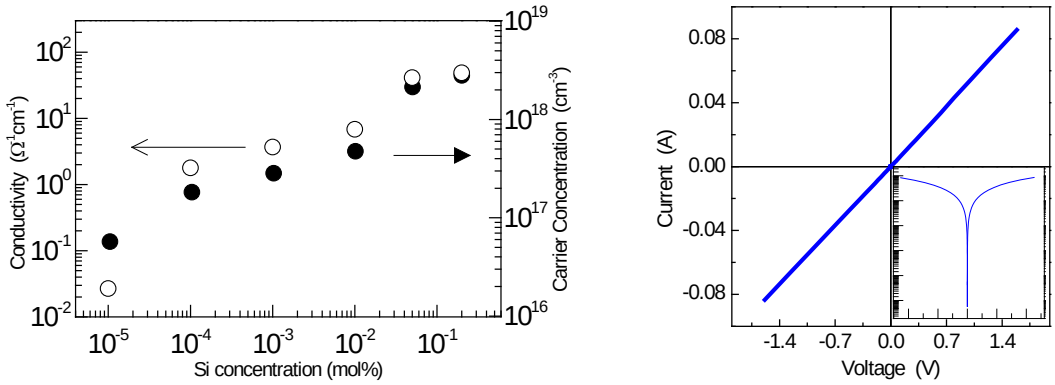

Figure 5. (left) Electrical conductivity and carrier concentration control by Si doping.[3] (right) *I-V* characteristic of Ti electrode on a β-Ga_2O_3 conductive wafer (in semilogarithmic scale in the inset).

In order to use β-Ga_2O_3 wafers as substrate, it is very important to have a precise control of the electrical properties. At the beginning it was thought that the n-type conductivity of β-Ga_2O_3 originates on oxygen vacancies that singly or doubly ionized act as donors. Actually, the systematical change in carrier concentration with the oxygen partial pressure of growth atmosphere has been assessed by many authors.[4–6] It has been found, however, that silicon, as main impurity present in Ga_2O_3 raw materials, may play also an important role. So, by intentional Si doping in crystals grown by the FZ technique it has been shown that the carrier

Table 1. β-Ga_2O_3 properties.

Melting point	1725℃
Density	5.95 g/cm^3
Linear expansion coefficients	<1 0 0>: 1.9×10^{-6} K^{-1}
(300 K - 1300 K)	<0 1 0>: 5.9×10^{-6} K^{-1}
	<0 0 1>: 5.9×10^{-6} K^{-1}
Thermal conductivity	$\perp$(1 0 0): 13.6 W/mK
	$\perp$(0 1 0): 22.8 W/mK
Specfic heat	0.49×10^3 J/kgK
Refractive index	1.97
Vickers hardness	($\bar{2}$ 0 1): 12.5 GPa
Effective n-type carrier concentration (by Si- or Sn-doping)	10^{16}-10^{19} cm^{-3}
Electron mobility	10-200 cm^2/Vs

concentration and conductivity can be controlled about three orders of magnitude[3] (Fig. 5 (left)). As the actual Si concentrations measured by the inductively coupled plasma (ICP) technique were below the nominal ones, it was deduced that a part of the dopant evaporated from the melt during the growth process. A similar doping behavior has been observed for Sn, however, due to the stronger SnO_2 evaporation from melt, the conductivity control is more difficult. Sn doping has been shown to be more practical in the case of molecular beam epitaxy (MBE) deposition.[7] On the other side, Mg and Fe doping are used to decrease the effective carrier concentration. In conclusion, thanks to the control of carrier concentration during the growth, semi-insulating and conductive β-Ga_2O_3 wafers are already commercially available (KOHA Co., Ltd. & Tamura Corp.).

The temperature dependence of the conductivity has been investigated by several authors.[5,8,9] The conductivity increases over one order of magnitude from helium to room temperature, but it doesn't follow a single activation mechanism.[8] The last important matter is the electrode for n-type wafers. Ti, in combination with Al or Au as oxidation protective layers, has been proved to provide a good Ohmic contact for n-type β-Ga_2O_3 samples[8] as shown in Fig. 5 (right). Later, the Ohmic characteristic of the Ti electrode can be improved by a prior Si ion-implantation. The latest reported specific contact resistance and resistivity are as low as 4.6×10^{-6} Ωcm^2 and 1.4×10^{-3} Ωcm, respectively.[10]

Table 1 summarizes some of the β-Ga_2O_3 properties. The thermal conductivity of β-Ga_2O_3 is in the order of 20 W/mK, which is very close to that of sapphire. The same applies for the Vickers hardness, which has a value of 12.5 GPa for the ($\bar{2}$ 0 1)-plane. Due to the monoclinic structure, β-Ga_2O_3 possesses two refractive indices which vary in a complex manner with the wavelength and polarization direction of light. Simplifying, in the visible wavelength region the refractive index is quite high, achieving a value near to 2.

2.2 β-Ga_2O_3 as substrate for high-brightness LEDs

Homoepitaxial growth of β-Ga_2O_3 was firstly demonstrated on the (1 0 0)-plane by RF-plasma-assisted MBE.[11] At present, ozone is utilized as oxygen source for MBE, since it provides a stable and reproducible gas flow.[7] Using this latter technique, it has been shown that the deposition rate depends strongly on the substrate orientation. The *a*-plane has the lowest deposition rate. This is caused by the low bonding character of the main cleavage plane. The deposition rate increases on *c*-plane, and it becomes more than ten times faster on *b*-plane. Therefore, the latter orientation is preferred for homoepitaxial growth in power devices (see section 2.3).

Due to the difference in crystal structure with other common semiconductors, the use of β-Ga_2O_3 as substrate wasn't considered for long time. The heteroepitaxial growth of GaN on β-Ga_2O_3 was firstly achieved by MBE after an effective nitridation process.[12–14] If the surface wasn't nitridized, only an inhomogeneous zincblende (1 1 1) GaN layer with low adhesivity was deposited on (1 0 0) β-Ga_2O_3 (Fig. 6 (left)). On the contrary, a wurtzite (0 0 1) GaN layer grew epitaxially on nitridized surfaces. The nitridation with ammonia, NH_3, starts to be effective at temperatures and pressures over 800℃ and 10^2 Pa, respectively. At that moment, the reflection

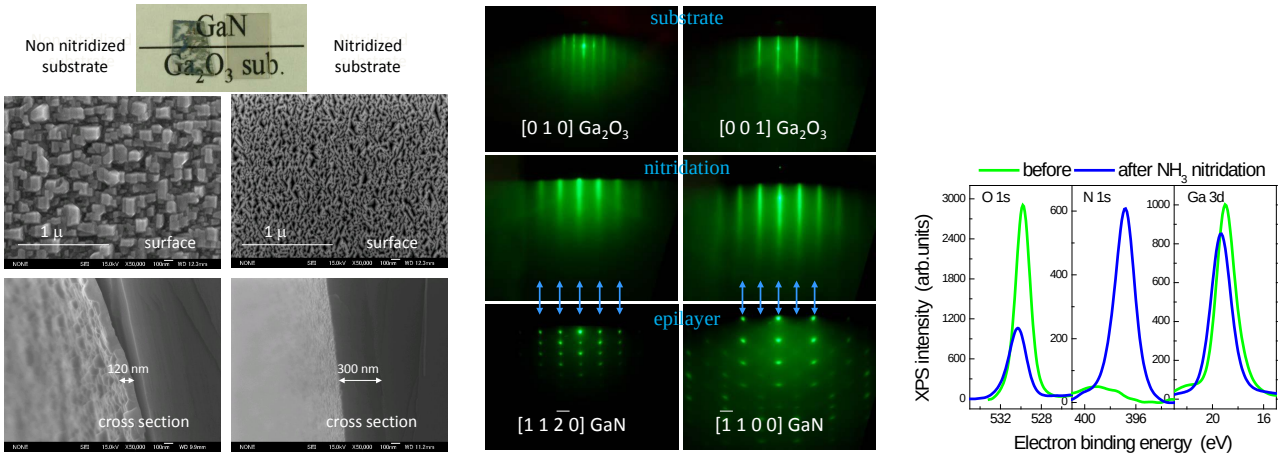

Figure 6. GaN heteroepitaxy on (1 0 0) β-Ga_2O_3 wafers by MBE. (left) Photograph and SEM images of two GaN layers grown on pristine and nitridized β-Ga_2O_3 substrates, respectively. (middle) RHEED patterns of substrate, before and after nitridation, and of wurtzite GaN during deposition. (right) XPS of a β-Ga_2O_3 wafer prior and after nitridation.

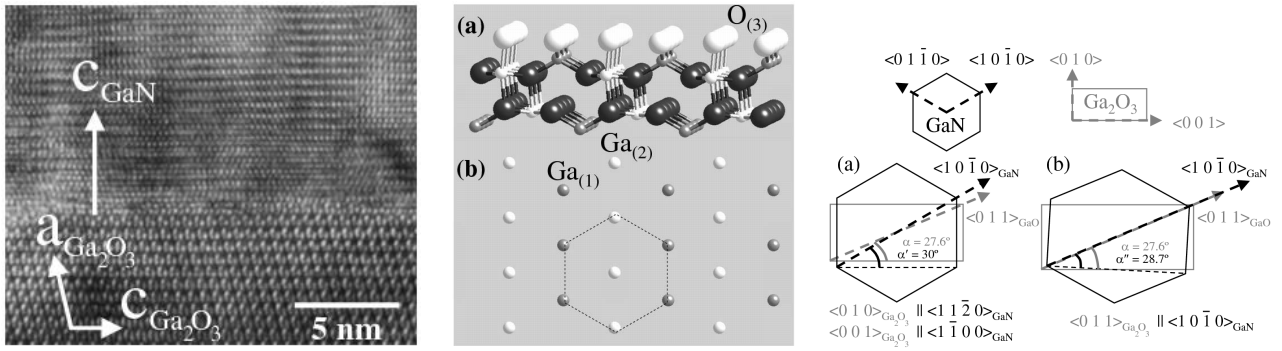

Figure 7. (left) TEM image of the GaN\β-Ga_2O_3 interface. (middle) Lattice view (a) perpendicular to the (1 0 0) plane of β-Ga_2O_3 and (b) the corresponding bird view of the first Ga atomic layer on (1 0 0) plane. (right) In-plane epitaxial relationship between (1 0 0) β-Ga_2O_3 and (0 0 1) wurtzite GaN.

high-energy diffraction (RHEED) patterns of the substrate change from 2- to 6-fold symmetry with a new lattice spacing that matches to GaN, as observed by the subsequent deposition of a GaN layer (Fig. 6 (middle)). X-ray photoelectron spectroscopy (XPS) carried out on only nitridized surfaces indicated that the upper oxygen layer had been substituted by a nitrogen layer (Fig. 6 (right)). This layer remained stable under air. Transmission electron spectroscopy (TEM) confirmed the existence of a smooth single layer interface (Fig. 7 (left)). The atomic model explaining this good lattice matching between both compounds is given in Fig. 7 (middle). The (1 0 0) surface is terminated with oxygen atoms, and if these are removed, the underlying Ga atoms are arranged in an almost regular hexagonal structure with interatomic distances very close to those of GaN. Therefore, when oxygen is substituted by nitrogen during the nitridation process, the upper surface reconstructs forming a GaN monolayer. The in-plane epitaxial relationship is illustrated in Fig. 7 (right). Although initial X-ray diffraction measurements pointed to the alignment along main directions, a more detailed study by TEM indicated the preferential alignment along the diagonal, which is only about 1 degree tilted from the initial assignment,[14] and has an approximated lattice mismatch of about 2.6%. At this point it should be noticed that for this configuration the in-plane lattice expansion of both β-Ga_2O_3 and GaN is very similar, so that the stress induced to the epitaxial layer during the cooling process to room temperature is minimal.

A few years have passed since the first demonstration of a blue-LED deposited on a (1 0 0) β-Ga_2O_3 FZ-wafer.[15] At present, ($\bar{2}$ 0 1) β-Ga_2O_3 EFG-wafers are used for the deposition of blue-emitting InGaN multi-

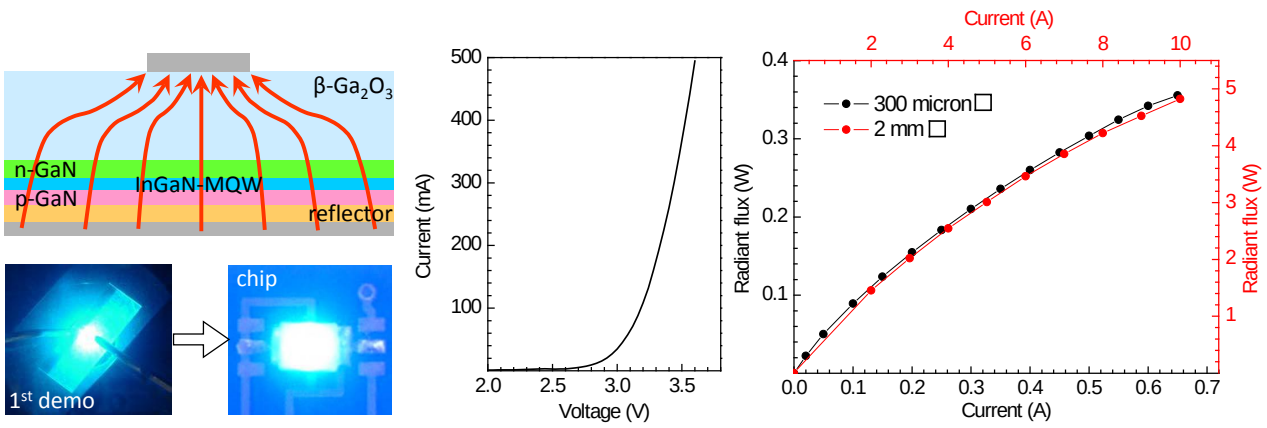

Figure 8. (left) Schematic of a blue-LED based on an InGaN-MQW deposited on a β-Ga_2O_3 substrate. Photograph of the initially demonstrated blue emission by vertical current injection in comparison with a current chip. (middle) *I-V* characteristic of a blue-LED on β-Ga_2O_3 substrate. (right) Radiant flux as a function of the vertical current flow for two different chip areas, 300 μm□ (left-down black coordinates) and 2 mm□ (up-right red coordinates), respectively. The radiant fluxes were measured with an integrating sphere.

quantum wells (MQWs) by a low-pressure MOCVD process.[16]In analogy with the (1 0 0) plane, the atomic arrangement of oxygen in this case, is very close to a regular hexagon. The deposition sequence at the interface utilized by KOHA Co., Ltd. & Tamura Corp. is as follows:[16]
(1) masking with a SiN_x layer to promote epitaxial lateral overgrowth and to drastically diminish the interface resistivity,
(2) low-temperature buffer layer between 400-550℃ to prevent reaction between β-Ga_2O_3 wafer surface and gases (H_2 and NH_3) above 600℃, and subsequent introduction of H_2 instead of N_2 in the gas-flow ,
(3) 1st GaN layer between 850-1030℃,
(4) 2nd GaN layer between 1050-1120℃.
The SiN_x layer is effective to reduce threading dislocations. On this template, a standard InGaN-MQW is deposited and electrodes are evaporated on the front and rear surfaces. The fabrication of such a vertically structured p-side-down LED is schematically illustrated in Fig. 8 (left). The light is extracted from the β-Ga_2O_3 wafer, due to its high visible transparency. The diode characteristic is shown in Fig. 8 (middle). For a blue emission peaking at 447 nm, the drive voltage at 20 mA is as low as 2.96 V. This indicates that the series resistance is lower than on other substrates and therefore the heat losses are notably suppressed. The radiant fluxes are given in Fig. 8 (right) as a function of the vertical current injection. Two types of chip sizes are considered, a small one, comparable to standard horizontal LEDs deposited on insulating sapphire, and a large one, which takes full advantage of the vertical current injection. The small area LED of 300 μm□ emits a radiant flux of 360 mW at 650 mA (left-down black coordinates). In contrast, the large area LED of 2 mm□ can provide a radiant flux of 4.82 W while supporting a current flow as large as 10 A (up-right red coordinates). These results demonstrate the realization of high-brightness blue-LED on β-Ga_2O_3 wafers, and point towards the competitive mass-production of these for general illumination purposes.

2.3 β-Ga_2O_3 for power devices

β-Ga_2O_3 possesses the largest bandgap among the transparent conductive oxides and this is surpassed only by diamond when compared with wide bandgap semiconductors in general. This property confers a unique potential for the next generation of high-power and high-voltage devices on β-Ga_2O_3, whereas a reduction in recovery losses, downsizing of passive filter components, and higher operating temperatures are demanded. A comparison of the major semiconductor materials is given in Table 2. The breakdown field of β-Ga_2O_3 has been estimated by the interpolation with other semiconductors,[17] obtaining a value as high as 8 MV/cm. The Baliga's figure of merit for power devices, which depends cubically on the breakdown field, was evaluated from these material properties. The estimated value for β-Ga_2O_3 is outstanding, being at least four times larger than

Table 2. Comparison of properties of major semiconductors.

Properties	Si	4H-SiC	GaN	Diamond	β-Ga_2O_3
Bandgap E_g (eV)	1.1	3.3	3.4	5.5	4.8
Electron mobility μ (cm^2/Vs)	1500	1000	1200	1800	300[a)]
Breakdown field E_b (MV/cm)	0.3	3.0	3.3	10	8[a)]
Dielectric constant ϵ_r	11.8	10	9.5	5.5	10
Baliga's figure of merit[b)]	1	570	860	21000	3200

a) Estimated.[7,17]
b) $\epsilon\mu E_b^3$ for DC and low frequency.

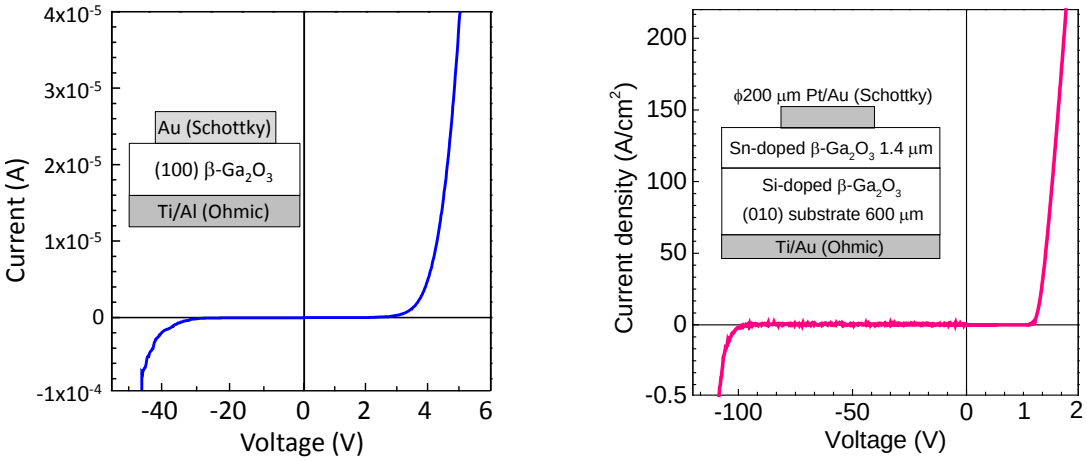

Figure 9. (left)I-V characteristic of the first Au/β-Ga_2O_3 Schottky barrier diode.[18] (right) I-V characteristic of a Pt/β-Ga_2O_3 Schottky barrier diode.[7]

those for GaN and 4H-SiC counterparts.

The first Schottky barrier diode (SBD) was reported on Au/β-Ga_2O_3. It exhibited a forward voltage of about 4 V and a ten times higher reverse breakdown voltage,[18] as seen in the I-V characteristic of Fig. 9 (left). This has been recently improved by using the structure shown schematically in Fig. 9 (right) together with the I-V characteristic. A high carrier concentration layer (1×10^{19} cm^{-3}) of 1.4 μm thickness was deposited homoepitaxially by MBE on a (0 1 0) β-Ga_2O_3 substrate. Pt/Au and Ti/Au contacts were deposited by electron-beam evaporation as Schottky and Ohmic contacts, respectively.[7] This SBD exhibited a forward voltage of 1.7 V (at 200 A/cm^2) and a reverse breakdown voltage as high as 100 V. The estimated on-resistance was 2 mΩcm^2. Therefore, a high breakdown voltage and a low on-resistance were achieved simultaneously. This is another important milestone that has made possible the realization of the first β-Ga_2O_3 based field-effect transistors (MESFET and MOSFET).[17,19,20] These devices exhibit already very promising properties: an ideal pinch-off of the drain current, a low off-state drain leakage leading to an on/off drain current ratio of about 10^{10}, and an off-state breakdown voltage of 370 V. Therefore, in the coming years a rising number of scientific works showing the performance and improvements on β-Ga_2O_3 power devices is expected.

3. SINGLE-CRYSTAL PHOSPHORS

There are four main ways to produce white LEDs: (a) UV-LED + blue-yellow-red phosphors, (b) blue-yellow-red LEDs, (c) blue-LED + yellow-red phosphor and (d) blue-LED + yellow phosphor. Depending on the application, the needs for color rendering (Ra), luminous efficiency of the source and stability vary. So, *e.g.* single LED + phosphor sources, emitting a cool white, are enough for backlights and indicators. For general illumination purposes, however, there is a strong demand to produce brighter and warmer sources at a moderate cost in order to be price competitive with currently used light bulbs, halogen and mercury-fluorescent lamps. Aiming

at this, great progress has been done in the development of blue-LED + yellow-red phosphors, emitting with correlated color temperatures (T_c) ranging between 3000 and 5000 K. More powerful white light sources can be obtained by LDs + phosphors. Relevant applications of these are automotive headlights, street illumination, and laser projectors, among others. So far, all phosphors are based on compounds in powder form, which are mainly synthesized by solid-state reaction and co-precipitation.[21] These powders need to be embedded in epoxy or silicone resins. In the case of high-brightness LEDs and LDs, the encapsulants require high physical and chemical stability in order to prevent aging processes, which affect not only the device brightness, but also the luminescent characteristics like *Ra* and T_c. The new concept proposed recently by our group[22] is shown schematically in Fig. 10 (left): Substitution of the phosphor-resin by a single-crystal phosphor. There are two main advantages in this approach. On the one hand, in comparison with powders, single-crystal phosphors can achieve the highest QEs due to the lack of grain boundaries and surface defects. On the other hand, the physical and chemical stabilities are better for the same reasons and due to the absence of organic resins. These two benefits are very important for white light application, particularly in the case of high-brightness light-sources.

3.1 Growth and properties of single-crystal phosphors

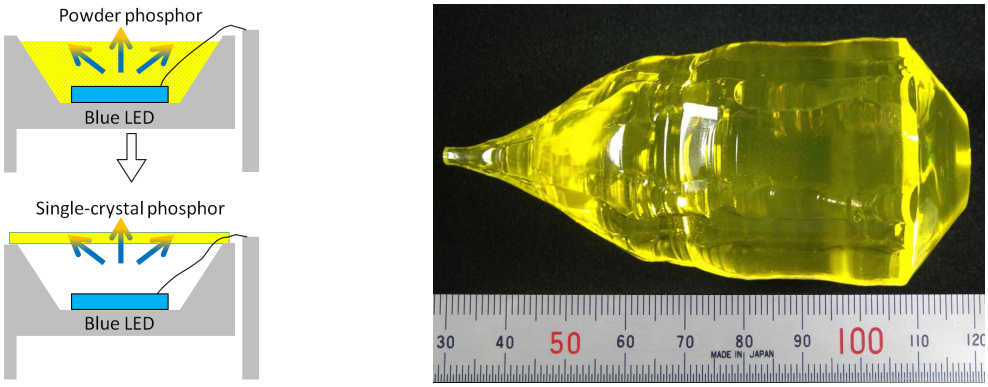

Figure 10. (left) Schematic of the new concept, where standard powder-phosphors embedded in a resin are substituted by a remote single-crystal phosphor. (right) Large-size Ce:YAG single-crystal phosphor grown by the Cz technique.

Ce-doped yttrium aluminum garnets are well known yellow-phosphors for the production of white light sources.[21] These crystals can be easily grown by the Cz-technique along the <1 1 1> axis and at common pulling and rotation rates, 1 mm/h and 10 rpm, respectively. Figure 10 (right) shows as an example a 2 inch in diameter Ce:$Y_3Al_5O_{12}$ (Ce:YAG) single crystal. This compound, which is chemically and physically highly stable, is the yellow phosphor par excellence for blue-LED excitation.

The excitation and emission spectra of Ce-doped garnets are characterized by two broad absorption bands in the UV and blue regions, and a very broad emission in the green-yellow. The latter is caused by the electron transition from the lowest excited 5d state ($^2D_{3/2}$) to the 4f ground states ($^2F_{5/2}$ and $^2F_{7/2}$), leading to two Gaussian emissions as can be seen in Fig. 11 (left). The positions of excitation and emission levels depend on the local crystal field, so that the luminescence characteristics can be adjusted by the engineering of the lattice. Gadolinium, which a larger ionic radius that increases the lattice parameter, is known to shift the Ce^{3+} emission to the red. On the contrary, lutetium doping leads to a green-shift.

Independently of the composition of the Ce-doped garnets, the internal QE measurements (determined by the relative absorption and emission intensities, *i.e.* emitted photons/absorbed photons) on single-crystals show that the QEs of these phosphors tend to increase with the temperature, reaching values close to the maximum (Fig. 11 (right)). Instead, reference powder phosphors, which also exhibit high internal QEs of about 95% at room temperature, suffer a decrease in efficiency at high temperatures. This drop in performance is attributed to the detrimental influence of defects present in commercial powder phosphors.

The novelty of single-crystal phosphors is evident for applications requiring high light-intensities. In these cases, the temperature of the devices increases significantly, and consequently the temperature of the phosphors

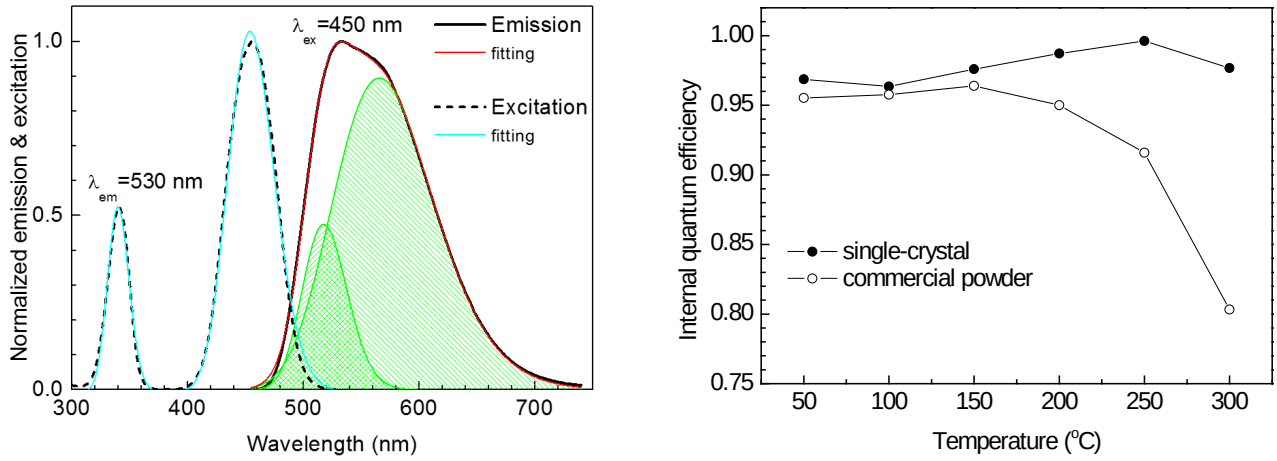

Figure 11. (left) Excitation and emission spectra from a yellow single-crystal phosphor. The curves are fitted by Gaussians, two for each spectrum. (right) Internal QE of a single-crystal phosphor in comparison with an equivalent commercial powder phosphor.

can also considerably rise. Therefore, the physical and chemical stability of single-crystal phosphors represents a clear advantage for this kind of applications.

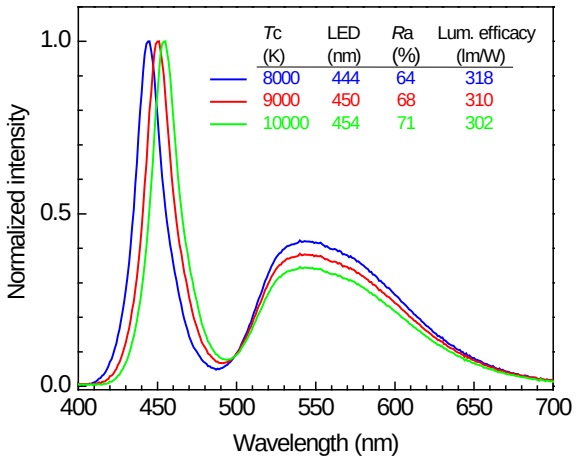

Figure 12. Simulated emission curves for cool white lights based on blue-LED + single-crystal Ce:YAG. The approximated standard illuminants are D80, D90 and D100.

Taking into account just a blue-LED and a single-crystal Ce:YAG phosphor, the color rendering and luminous efficacy at 100℃ have been simulated for three standard cool white illuminants, namely D80, D90 and D100. As can be seen in Fig. 12, T_c and *Ra* increase as the blue-LED emission shifts to longer wavelengths and the phosphor intensity decreases.

In order to obtain warm white light-sources, the addition of a red-phosphor is required. For comparison, the *Ra* and the luminous efficacy at 100℃ have been estimated as a function of the blue-LED and the yellow single-crystal phosphor emissions, while fixing the red phosphor emission at 645 nm. Figure 13 (left) indicates that *Ra* values over 90 are achievable in a wide range. A maximum of 97 is obtained at 454 and 520 nm for blue and yellow emissions, respectively. The simulated spectrum of the three components at the maximum has a luminous efficacy of 277 lm/W and it is shown in Fig. 13 (right).

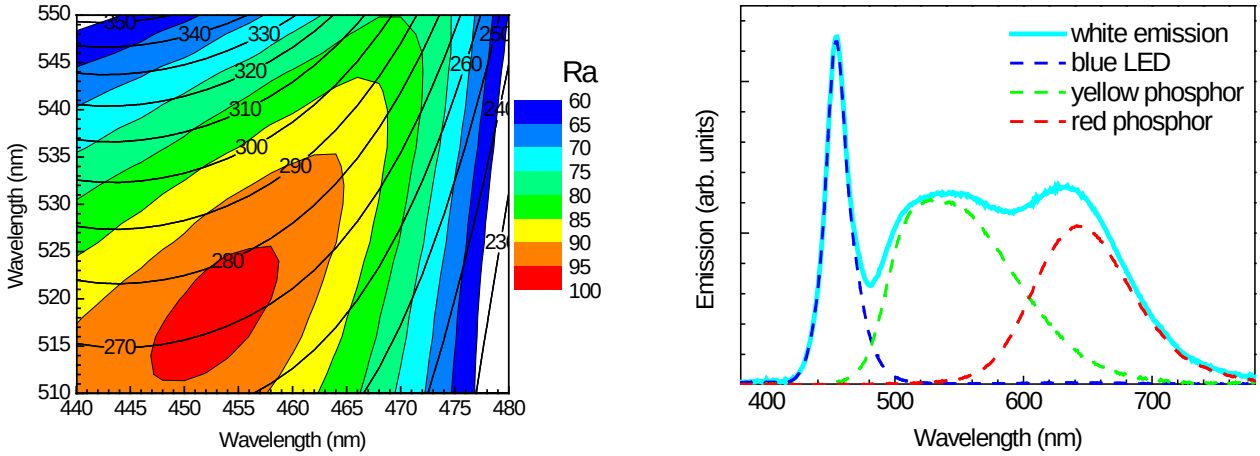

Figure 13. (left) General color-rendering index Ra and luminous efficacy (lm/W) of T_c=5000 K white LEDs as a function of the blue-LED and yellow single-crystal phosphor emission maxima, and using a red phosphor emitting at 645 nm. (right) Simulated emission curve for the highest Ra=97 at 454 and 520 nm. The corresponding luminous efficacy is 277 lm/W.

4. CONCLUSIONS

The growth of high-quality β-Ga_2O_3 single-crystals by the EFG technique is proved. In comparison with other materials like GaN and SiC, which need to be synthesized from the solution at high pressure or from the vapor phase, the growth of β-Ga_2O_3 from the melt by the EFG technique is very advantageous. The crystals can be grown at high speed (10-30 mm/h), at the convenient pressure of one atmosphere, and with the desired industrial size, since the EFG is a comparatively easy scalable technique. These facts favor in turn low production costs, thus price-competitive wafers for the production of LEDs, LDs, power devices, solar blind sensors and others, are feasible.

The performance of high-brightness vertically structured blue-LEDs (InGaN-MQW on β-Ga_2O_3 substrate, p-side-down) is demonstrated. By the vertical injection, the current crowding inherent to horizontal structures is avoided, the heat is dissipated more efficiently, and also the forward operation voltage decreases, thus also the heat losses are diminished. The light comes out through the substrate, taking advantage of its high transparency. Continuous improvements are expected by the further decreasing of series resistance and the enhancement of light extraction efficiency.

The estimated Baliga's figure of merit for β-Ga_2O_3 power devices is significantly larger than those of GaN and 4H-SiC wide bandgap counterparts. The performance of initial β-Ga_2O_3 transistors lets envisage a bright future for the next generation of high-power high-voltage applications.

At last, a new approach for light conversion using single-crystal phosphors has been introduced. In comparison with currently used commercial phosphors, single-crystal phosphors avoid the use of resins, exhibit a bit higher internal QEs, and most of all, a higher temperature stability. Therefore, these are very promising for white light applications, in particular for those involving high-brightness LEDs or LDs as primary light sources.

ACKNOWLEDGMENTS

REFERENCES

[1] Geller, S., "Crystal Structure of β-Ga_2O_3," *J. Chem. Phys.* **33**, 676 (1960).

[2] Víllora, E. G., Shimamura, K., Yoshikawa, Y., Aoki, K., and Ichinose, N., "Large-size β-Ga_2O_3 single crystals and wafers," *J. Cryst. Growth* **270**, 420–426 (2004).

[3] Víllora, E. G., Shimamura, K., Yoshikawa, Y., Ujiie, T., and Aoki, K., "Electrical conductivity and carrier concentration control in β-Ga_2O_3 by Si-doping," *Appl. Phys. Lett.* **92**, 202120 (2008).

[4] Víllora, E. G., Morioka, Y., Atou, T., Sugawara, T., Kikuchi, M., and Fukuda, T., "Infrared Reflectance and Electrical Conductivity of β-Ga_2O_3," *Phys. Stat. Sol.(a)* **193**, 187–195 (2002).

[5] Yamaga, M., Víllora, E. G., Shimamura, K., and Ichinose, N., "Donor structure and electric transport mechanism in β-Ga_2O_3," *Phys. Rev. B* **68**, 155207 (2003).

[6] Ueda, N., Hosono, H., Waseda, R., and Kawazoe, H., "Synthesis and control of conductivity of ultraviolet transmitting β-Ga_2O_3 single crystals," *Appl. Phys. Lett.* **70**, 3561 (1997).

[7] Sasaki, K., Kuramata, A., Masui, T., Víllora, E. G., Shimamura, K., and Yamakoshi, S., "Device-Quality β-Ga_2O_3 Epitaxial Films Fabricated by Ozone Molecular Beam Epitaxy," *Appl. Phys. Express* **5**, 35502 (2012).

[8] Víllora, E. G., Shimamura, K., Ujiie, T., and Aoki, K., "Electrical conductivity and lattice expansion of β-Ga_2O_3 below room temperature," *Appl. Phys. Lett.* **92**, 202118 (2008).

[9] Orita, M., Ohta, H., and Hirano, M., "Deep-ultraviolet transparent conductive β-Ga_2O_3 thin films," *Appl. Phys. Lett.* **77**, 4166 (2000).

[10] Sasaki, K., Higashiwaki, M., Kuramata, A., Masui, T., and Yamakoshi, S., "Si-Ion Implantation Doping in β-Ga_2O_3 and its Application to Fabrication of Low-Resistance Ohmic Contacts," *Appl. Phys. Express* **6**, 086502 (2013).

[11] Víllora, E. G., Shimamura, K., Kitamura, K., and Aoki, K., "Rf-plasma-assisted molecular-beam epitaxy of β-Ga_2O_3," *Appl. Phys. Lett.* **88**, 031105 (2006).

[12] Víllora, E. G., Shimamura, K., Aoki, K., and Ichinose, N., "Reconstruction of the β-Ga_2O_3 (1 0 0) cleavage surface to hexagonal GaN after nitridation," *J. Cryst. Growth* **270**, 462–468 (2004).

[13] Víllora, E. G., Shimamura, K., Aoki, K., and Kitamura, K., "Molecular beam epitaxy of *c*-plane wurzite GaN on nitridized *a*-plane β-Ga_2O_3," *Thin Solid Films* **500**, 209–213 (2006).

[14] Víllora, E. G., Shimamura, K., Kitamura, K., Aoki, K., and Ujiie, T., "Epitaxial relationship between wurzite GaN and β-Ga_2O_3," *Appl. Phys. Lett.* **90**, 234102 (2007).

[15] Shimamura, K., Víllora, E. G., Domen, K., Yui, K., Aoki, K., and Ichinose, N., "Epitaxial Growth of GaN on (1 0 0) β-Ga_2O_3 substrates by Metalorganic Vapor Phase Epitaxy," *Jpn. J. Appl. Phys.* **4**, L7–L8 (2005).

[16] Kuramata, A., "Ga_2O_3 Crystal and its LED application," *Bull. Solid State Phys. Appl., (Jpn. Soc. Appl. Phys.)* **19**, 42 (2013). (in Japanese).

[17] Higashiwaki, M., Sasaki, K., Kuramata, A., Masui, T., and Yamakoshi, S., "Gallium oxide Ga_2O_3 metal-semiconductor field-effect transistors on single-crystal β-Ga_2O_3 (010) substrates," *Appl. Phys. Lett.* **100**, 013504 (2012).

[18] Shimamura, K., Víllora, E. G., and Aoki, K., "Characteristics of a Schottky diode using gallium oxide," *The 56th JSAP Spring Meeting*, 1a–E–4 (2009).

[19] Sasaki, K., Higashiwaki, M., Kuramata, A., Masui, T., and Yamakoshi, S., "MBE grown Ga_2O_3 and its power device applications," *J. Cryst. Growth* **378**, 591–595 (2013).

[20] Higashiwaki, M., Sasaki, K., Kamimura, T., Wong, M. H., Krishnamurthy, D., Kuramata, A., Masui, T., and Yamakoshi, S., "Depletion-mode Ga_2O_3 metal-oxide-semiconductor field-effect transistors on β-Ga_2O_3 (010) substrates and temperature dependence of their device characteristics," *Appl. Phys. Lett.* **103**, 123511 (2013).

[21] Chen, L., Lin, C., Yeh, C., and Liu, R., "Light Converting Inorganic Phosphors for White Light-Emitting Diodes," *Materials* **3**, 2172–2195 (2010).

[22] Latynina, A., Watanabe, M., Inomata, D., Aoki, K., Sugahara, Y., Víllora, E. G., and Shimamura, K., "Properties of Czochralski grown Ce,Gd:$Y_3Al_5O_{12}$ single crystal for white light-emitting diode," *J. Alloy. Compd.* **553**, 89–92 (2013).